

# Quantum Monte Carlo simulation of thin magnetic films

P. Henelius,<sup>1,\*</sup> P. Fröbrich,<sup>2,3</sup> P.J. Kuntz,<sup>2</sup> C. Timm,<sup>3</sup> and P.J. Jensen<sup>3,4</sup>

<sup>1</sup>*Condensed Matter Theory, Royal Institute of Technology, SE-106 91 Stockholm, Sweden*

<sup>2</sup>*Hahn-Meitner-Institut Berlin, Glienicke Straße 100, 14109 Berlin, Germany*

<sup>3</sup>*Institut für Theoretische Physik, Freie Universität Berlin, Arnimallee 14, 14195 Berlin, Germany*

<sup>4</sup>*Laboratoire de Physique Quantique, Université Paul Sabatier,*

*UMR 5626 du CNRS 118, route de Narbonne, F-31062 Toulouse, France*

(Dated: November 2, 2018)

The stochastic series expansion quantum Monte Carlo method is used to study thin ferromagnetic films, described by a Heisenberg model including local anisotropies. The magnetization curve is calculated, and the results compared to Schwinger boson and many-body Green's function calculations. A transverse field is introduced in order to study the reorientation effect, in which the magnetization changes from out-of-plane to in-plane. Since the approximate theoretical approaches above differ significantly from each other, and the Monte Carlo method is free of systematic errors, the calculation provides an unbiased check of the approximate treatments. By studying quantum spin models with local anisotropies, varying spin size, and a transverse field, we also demonstrate the general applicability of the recent cluster-loop formulation of the stochastic series expansion quantum Monte Carlo method.

PACS numbers: 75.10.Jm, 75.40.Mg, 75.70.Ak, 75.30.Gw

## I. INTRODUCTION

The driving force behind much of the research on thin magnetic films is their application in data storage devices. Magnetic thin films also display many remarkable physical phenomena, such as the reorientation effect,<sup>1</sup> in which the axis of magnetization changes as a function of film thickness, temperature and applied fields. Many theoretical methods, such as ab-initio calculations,<sup>2</sup> mean-field theories,<sup>3,4</sup> classical Monte Carlo simulations,<sup>5,6</sup> Green's function methods<sup>7,8,9,10,11,12</sup> and Schwinger bosons<sup>13</sup> have been applied to thin-film systems. Much of this work has focused on using the Heisenberg model to study the reorientation effect. The ground state and the lowest (one-magnon) excitations are known for the two-dimensional ferromagnetic Heisenberg model, but there is no closed form analytic solution at finite temperatures. Since results obtained using different approximate methods differ a great deal from each other, there is a need for an unbiased check of the various methods used; this is achieved by quantum Monte Carlo (QMC) calculations. In Ref. 8, for example, it has been shown by comparing with QMC results<sup>14,15</sup> that the Tyablicov<sup>16</sup> decoupling (random phase approximation: RPA) is a very good approximation for the magnetization of a spin  $S = 1/2$  monolayer in an external magnetic field (perpendicular to the film plane). The main purpose of the present paper is to show the feasibility of large-scale quantum Monte Carlo (QMC) calculations, free of systematic errors, in the study of thin magnetic films. In order to achieve this goal we have included higher spins, local anisotropies, and a transverse magnetic field in the operator-loop formulation of the stochastic series expansion (SSE) QMC method.<sup>17</sup>

Two often-cited trends in quantum Monte Carlo development are the emergence of methods free of system-

atic errors,<sup>15,18,19,20,21</sup> and the development of highly efficient loop-cluster algorithms.<sup>17,19,20,22,23,24</sup> In this work we particularly want to emphasize the *general applicability* of the SSE operator-loop method, which makes it possible to use the same algorithm to study a wide variety of Hamiltonians. Whereas previously it was necessary to rewrite large sections of the computer code when changing the model, one can now use the same code (compiled only once) to simulate a wide range of different systems. The user of the program no longer necessarily needs detailed knowledge of the algorithm and code to be able to conduct a thorough study of many quantum spin models in any dimension with, for example, non-zero magnetic fields, anisotropies and varying spin size.

A brief description of the QMC method is given in Sec. II. Thereafter we discuss the applicability of the method and the introduction of general spin size and a transverse field in the SSE operator-loop algorithm. In Sec. III we compare some examples of the QMC simulations to approximate theoretical approaches. Finally, we comment on possible future applications of QMC in the context of thin magnetic films.

## II. SSE CLUSTER-LOOP ALGORITHM

There are excellent descriptions of the SSE loop algorithm,<sup>17,24</sup> so we only give a brief summary here in order to introduce the general framework of the method. We will, however, try to describe the main features of the method pictorially. The focus is on the new aspects that arise when introducing arbitrary spin size and a transverse field.

We consider a lattice spin model described by a Hamiltonian  $H$ . The SSE method relies on a Taylor expansion

of the partition function  $Z$ :

$$Z = \sum_{\alpha} \sum_{n=0}^{\infty} \frac{(-\beta)^n}{n!} \langle \alpha | H^n | \alpha \rangle, \quad (1)$$

where  $|\alpha\rangle$  are basis states in which the matrix element above can be evaluated, and  $\beta$  is the inverse temperature.

To describe the updating procedure, we write the Hamiltonian as a sum over all  $M$  bonds representing interacting spins in the system

$$H = - \sum_{b=1}^M H_b. \quad (2)$$

The bond operator  $H_b$  can be decomposed into its diagonal and off-diagonal parts,

$$H_b = H_{D,b} + H_{O,b}, \quad (3)$$

where subscript  $D$  denotes a diagonal operator and  $O$  an off-diagonal operator. For a ferromagnetic Heisenberg model these two operators are of the form

$$-H_{D,b} = S_{i(b)}^z S_{j(b)}^z \quad (4)$$

and

$$-H_{O,b} = S_{i(b)}^+ S_{j(b)}^- + S_{i(b)}^- S_{j(b)}^+, \quad (5)$$

where  $i(b)$  and  $j(b)$  denote the two spins connected by bond  $b$ . If we introduce a cutoff order  $L$  in the Taylor expansion (which, when done properly, does not cause any systematic errors<sup>24</sup>), and include additional unit operators  $I$ , the expansion can be rewritten in the form

$$H = \sum_{\alpha} \sum_{S_L} \frac{\beta^n (L-n)!}{L!} \langle \alpha | S_L | \alpha \rangle, \quad (6)$$

where  $S_L$  is an operator string

$$S_L = \prod_{p=1}^L H_p, \quad (7)$$

with  $H_p \in \{H_{D,b}, H_{O,b}, I\}$ . The Monte Carlo procedure must sample the space of all states  $|\alpha\rangle$  and all operator sequences  $S_L$ .

We next consider the SSE space in more detail. Denoting a propagated state by

$$|\alpha(p)\rangle = \prod_{i=1}^p H_i |\alpha\rangle, \quad (8)$$

the matrix element in Eq. (6) can be written as a product of elements of the form  $\langle \alpha(p) | H_b | \alpha(p-1) \rangle$ , where the bond-operator  $H_b$  only acts on two spins. For the spin-1/2 Heisenberg model the only elements that can appear are  $\langle \uparrow, \uparrow | H_b | \uparrow, \uparrow \rangle$ ,  $\langle \uparrow, \downarrow | H_b | \uparrow, \downarrow \rangle$ ,  $\langle \uparrow, \downarrow | H_b | \downarrow, \uparrow \rangle$ , and the spin-reversed versions of the same set. From now on

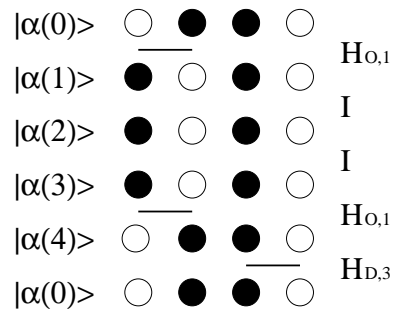


FIG. 1: An SSE configuration for a four-site spin-1/2 model. A filled (empty) circle denotes a state with spin up (down). A horizontal bar indicates a vertex, corresponding to a bond operator  $H_b$ , labeled on the right. The propagated states  $|\alpha(p)\rangle$  are labeled on the left side.

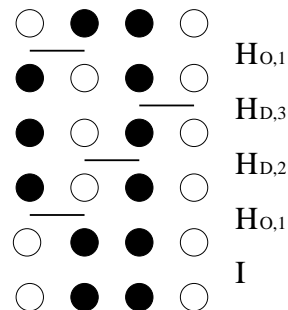


FIG. 2: A possible outcome of performing a diagonal update on the configuration in Fig. 1.

we refer to these matrix elements, consisting of four spin states and a bond operator, as “vertices”. The matrix element in Eq. (6) can thus be viewed as a list of vertices of the above kind. In Fig. 1 we depict such a list graphically.

In the operator-loop algorithm, two basic updates ensure that the complete SSE space is sampled. The diagonal update attempts to exchange diagonal operators  $H_{D,b}$  and unit operators  $I$ . The probability for inserting a diagonal operator (exchanging it for a unit operator) at position  $p$  in the operator sequence is

$$P_{\text{insert}} = \frac{M\beta \langle \alpha(p) | H_{D,b} | \alpha(p) \rangle}{L-n}, \quad (9)$$

while the probability for removing a diagonal operator is

$$P_{\text{remove}} = \frac{L-n+1}{M\beta \langle \alpha(p) | H_{D,b} | \alpha(p) \rangle}. \quad (10)$$

In a diagonal update, one exchange attempt is made for each diagonal and unit operator. A typical outcome of a diagonal update is shown in Fig. 2.

The second type of update is a global operator-loop update, which leaves unit operators unaffected. The idea of the loop move is to form and flip a closed loop of spins in the vertex list. In the process both the affected vertices and states are changed. The operator-loop update

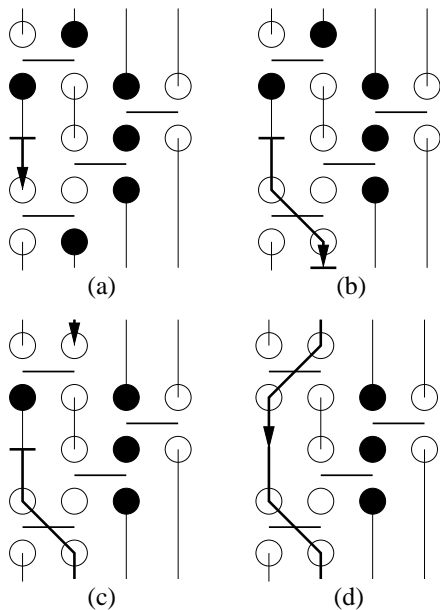


FIG. 3: A loop update. Unit operators have been removed from the configuration in Fig. 2. Vertical lines (links) show how the spins at different vertices are connected. Short horizontal bars denote link-discontinuities.

together with the above diagonal update ensure that the complete SSE configuration space is sampled.

The loop move is easy to formulate. In Fig. 3 we illustrate a loop move graphically. We have removed all the unit operators  $I$  from the operator sequence in Fig. 2. Furthermore we only show the spins that are members of a vertex, and we turn the configuration into a linked list by connecting the same spin at different vertices by vertical lines, which we refer to as “links”. Next we describe the loop move in more detail.

First a random spin, belonging to a vertex, is selected and flipped, see Fig. 3(a). We refer to this spin as the “entrance” spin to the first vertex. For the loop to proceed, we select an “exit” spin, also belonging to the same vertex, see Fig. 3(b). The probability of choosing a given exit spin is proportional to the vertex matrix element, that results from flipping the entrance and exit legs. This choice of exit spin ensures detailed balance.<sup>24</sup> The exit spin is linked to another spin in the linked vertex list, and this spin is chosen as the entrance spin to the next vertex, see Fig. 3(c). In this manner a loop of spins on the space-time lattice is formed and flipped. Note that when the first spin is flipped a discontinuity is introduced into the vertex list. A link-discontinuity appears when two spins linked together are not in the same state. When, for example, the initial entrance and exit spins (assuming they are different) are flipped, two discontinuities are introduced in the linked list, see Fig. 3(b), where a link-discontinuity is marked by a short horizontal bar. One of the discontinuities gets propagated by the loop until the loop passes through the initial spin a second time, when the discontinuities “annihilate” each other and the loop

closes, see Fig. 3(d). A practical and sufficient criterion for closing the loop is that the exit spin (after having been flipped) is in the same state as the next entrance spin (before flipping it). When this is the case, all discontinuities have been removed and the loop can be closed.

### A. Applicability of the algorithm

The SSE loop algorithm is extremely general and can be efficiently applied to any model with a positive definite partition function (if this is not the case, one encounters the usual difficulties due to the sign problem<sup>25</sup>). This means that the algorithm can be applied to ferromagnetic and antiferromagnetic (on bipartite lattices) Heisenberg models of any quantum spin size in any dimension, including magnetic fields and local as well as exchange anisotropies. The interactions need not be short-ranged, as long as they do not cause frustration (which leads to the sign problem).

From a programming point of view, one need only calculate the energies of all possible vertices (which typically is a simple task) and generate a table of exit probabilities as a function of four variables: the initial vertex type, the entrance spin, the entrance spin state and the exit spin.

As an illustration we have written a code that works for a general  $d$ -dimensional Heisenberg model of the form

$$\begin{aligned}
 H = & - \sum_{ij} [J_{ij}^z S_i^z S_j^z + J_{ij}^t (S_i^+ S_j^- + S_i^- S_j^+)] \\
 & - \sum_i [K_2 (S_i^z)^2 + K_4 (S_i^z)^4] \\
 & - \sum_i [B^z S_i^z + B^x S_i^x], \quad (11)
 \end{aligned}$$

where the exchange interaction is given by  $J_{ij}$  (negative for antiferromagnets and positive for ferromagnets).  $\mathbf{S}$  denotes the quantum spin and  $K_2$  and  $K_4$  are the second and fourth-order local uniaxial anisotropies.  $\mathbf{B}$  is an external magnetic field. In this study we limit ourselves to a nearest neighbour interaction, but in principle one can include long-range interactions. In the following we describe the modifications to the loop algorithm that allow the introduction of general spin size and a transverse field.

### B. Inclusion of arbitrary spin

For the sake of simplicity, the SSE loop-operator algorithm was originally described<sup>17</sup> for a spin-1/2 system, but the generalization to a spin- $S$  system is straightforward. For an arbitrary spin system there are more allowed vertices, but the probability for inserting and extracting diagonal operators is still given by Eq. (9) and Eq. (10) respectively. The only necessary change in the loop-update is the choice of the initial spin state. For

the spin-1/2 model the initial entrance spin was simply flipped, but for the spin- $S$  model one can randomly choose among the  $2S$  spin states that differ from the initial spin state. All other aspects of the algorithm remain the same.

### C. Inclusion of a transverse field

Previously a transverse field has been included in the SSE algorithm using local updates.<sup>15</sup> In the present work we include the transverse field directly in the global loop update. There are very likely many different ways to formulate a loop-update which includes a transverse magnetic field. Here we will not make an exhaustive study, but rather present one possible algorithm, which we found particularly simple to implement. It is probably not the most efficient update, and we are currently making a more detailed study of more efficient algorithms for including the transverse field.

Including a transverse magnetic field is more involved because the total  $z$  component of the magnetization is no longer a conserved quantity,  $[H, \sum_i S_i^z] \neq 0$ , due to the presence of single lowering and raising operators ( $2S^x = S^+ + S^-$ ) in the Hamiltonian. As a consequence additional “flip vertices”, with different magnetization in the initial and final states (such as  $(\uparrow, \uparrow | H_b | \uparrow, \downarrow)$ ), are also allowed in the vertex-list. The presence of flip vertices implies that, in general, one can exit the same exit spin with several different spin states. The increase in the number of exit states means that the exit probability is a function of five variables instead of four: original vertex, entrance spin, entrance state, exit spin and exit state. For a model that conserves the total  $z$  component of the magnetization the exit state is a function of the other four variables.

To include a magnetic field, we also have to reconsider how to start, and end, the operator-loop. With no magnetic field we introduce an initial link-discontinuity by flipping the first entrance spin. A second link-discontinuity appears when the first exit spin is flipped (unless the entrance and exit spins coincide, in which case the loop closes immediately). The second discontinuity is propagated as the loop progresses until the two discontinuities annihilate each other and the loop closes. With flip vertices allowed, the number of link-discontinuities can change by the introduction or removal of single flip vertices. If one therefore chooses to start, and end, the loop in the same way as previously described, the loop can close without having corrected for the initial discontinuity. In such a case it would be necessary to return to the starting point of the loop and continue execution until the last discontinuity is removed.

Here we chose a slightly different approach, which can be implemented by a very minor change in the original formulation. Instead of picking an initial entrance spin and changing its state we leave its state *unchanged*. Without a magnetic field the loop would close immedi-

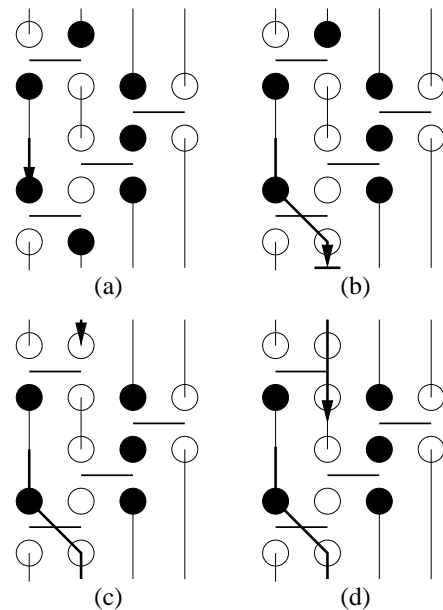


FIG. 4: A loop update in the presence of a transverse field. Note that there is no initial link-discontinuity, since the state of the initial spin in (a) is left unchanged. With a transverse field the first and last spins in the loop do not necessarily coincide.

ately. With a magnetic field this possibility still exists, but the loop may also start with a flip vertex and thereafter proceed in a “normal” fashion until another flip vertex is inserted, or removed, when the loop is closed according to the usual criterion (the exit spin and the following entrance spin are in the same state). We have compared high-precision QMC data for small systems with exact diagonalization, to ensure that detailed balance is indeed satisfied, but we do not provide a strict proof here.

Fig. 4 depicts an example of a loop move for the case of a non-zero transverse field. In Fig. 4(a) an initial entrance spin is selected and left in its original state. An exit spin is selected and flipped (Fig. 4(b)), resulting in a flip vertex. The next entrance spin can be seen in Fig. 4(c), with a corresponding exit spin in Fig. 4(d). Note that the exit state in Fig. 4(d) is unchanged, resulting in a second flip vertex, leading to termination of the loop. The loop does not close on itself in this case, but starts and ends at two different spins.

The transverse magnetization is particularly easy to calculate within the SSE formulation, since it simply is equal to the average number of flip vertices,  $N_{\text{flip}}$ , in the operator sequence,<sup>15</sup>

$$M_x = \frac{1}{\beta} \langle N_{\text{flip}} \rangle. \quad (12)$$

To conclude this section we note that only two changes need to be made to add a transverse field. First of all the initial entrance spin state should be left unchanged. Secondly, the exit probability is now also a function of

exit state, since there are, in general, several possible exit states for a given exit spin. Next we apply this algorithm to a two-dimensional ferromagnetic system.

### III. APPLICATION TO THIN MAGNETIC FILMS

The simplest effective model for a thin magnetic film is a ferromagnetic Heisenberg monolayer. However, the Mermin-Wagner theorem<sup>26</sup> tells us that this model cannot have a finite critical temperature in two dimensions. The continuous symmetry can be explicitly broken by an anisotropy in order to induce a finite critical temperature. Typical experimentally observed values of the local anisotropy in 3*d* transition metal films are about two orders of magnitude smaller than the exchange coupling, and one might therefore expect a very small critical temperature. However, it turns out that the critical temperature contains a logarithmic dependence on the anisotropy,<sup>5,13,27</sup> so that very small anisotropies induce a critical temperature of the order of the coupling constant. In this section we concentrate on results for the magnetization as a function of temperature. The model is given by Eq. (11), where the double sum is over all nearest neighbours on a two-dimensional square lattice. Since the main purpose of the present paper is to show the feasibility of the quantum Monte Carlo method, and not to explore the whole parameter range of the model as defined in Eq. (11), we limit ourselves to some illustrative examples. From now on we will assume an isotropic exchange interaction ( $J_{ij}^x = J_{ij}^y = J_{ij}^z/2$ ), zero vertical magnetic field ( $B^z = 0$ ) and only second-order anisotropy ( $K_4 = 0$ ). First we discuss how the finite-size effects were treated. Thereafter we compare the QMC results with approximate theoretical approaches. Finally, we also show a case where a transverse field drives the magnetization in the plane.

#### A. Finite-size effects

The first problem one encounters in a finite-size system with spin-inversion symmetry is that the magnetization should vanish because opposite spin orientations occur equally likely. One can circumvent this problem by calculating either the absolute value of the magnetization, or the magnetization squared (and take the root afterwards). Both approaches are equivalent in the thermodynamic limit, and, since the absolute value of the magnetization is found to converge faster, we show only the former. The magnetization curves for a particular value of the anisotropy,  $K_2/J = 0.01$ , and different system sizes are shown in Fig. 5. The finite-size effects increase closer to the Curie temperature  $T_c$ , as expected for a second-order phase transition. For low temperatures, however, one can see that it is possible to extract data which have converged (within statistical error) with

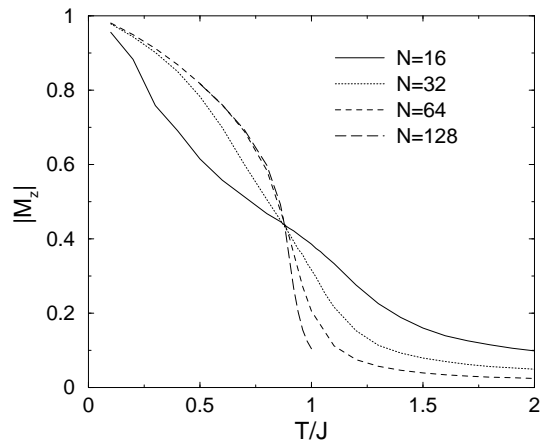


FIG. 5: Magnetization as a function of linear system size  $N$  and temperature  $T/J$  for  $S = 1$  and  $K_2/J = 0.01$ .

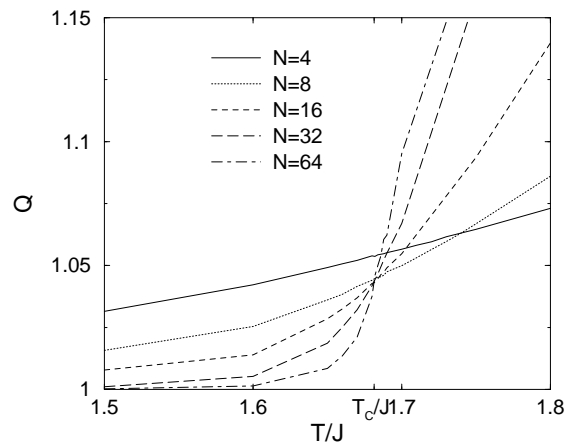


FIG. 6: The Binder ratio  $Q$  as a function of linear system size  $N$  and temperature  $T/J$  for  $S = 1$ , and  $K_2/J = 1.5$ .

respect to system size. In the next section we restrict ourselves to results for the magnetization that show no discernible finite-size effects.

The critical temperature can be determined directly. We have used the Binder ratio<sup>28</sup> to extract the value of  $T_c$ . By plotting the ratio of two moments of the magnetization,

$$Q = \frac{\langle M_z^4 \rangle^{\frac{1}{4}}}{\langle M_z^2 \rangle^{\frac{1}{2}}}, \quad (13)$$

the finite-size effects around  $T_c$  should largely cancel, and curves for different system sizes are expected to intersect at  $T_c$ . In Fig. 6 we show an example for  $K_2/J = 1.5$ , where one can clearly see how data for different system sizes intersect at one point ( $T_c/J$ ).

In transition-metal thin films, the second-order anisotropy is believed to be of the order  $K_2/J = 0.01$ . The relatively small energy scale of the anisotropy induces large finite-size effects. In order to see the effects

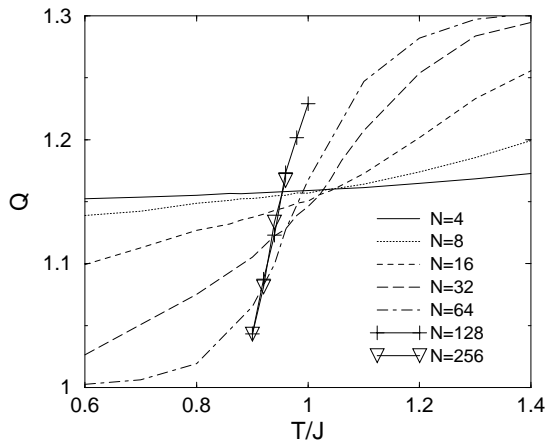


FIG. 7: The Binder ratio  $Q$  as a function of linear system size  $N$  temperature  $T/J$  for  $S = 1$  and  $K_2/J = 0.01$ .

of a small energy scale one needs to examine large systems at low temperatures. In Fig. 7 we show the Binder ratio as a function of temperature and system size for  $K_2/J = 0.01$ . It seems that results for linear system sizes  $N = 4, 8$  and  $16$  have converged around  $T_c/J \cong 1.05$ , but as the system size is increased strong corrections appear and push  $T_c/J$  down to around  $T_c/J \cong 0.9$ . This is a clear case where it would be dangerous to draw conclusions from a study of small system sizes. The results for system size  $N = 256$  have statistical errors which are slightly larger than the symbol size, while all other statistical errors are much smaller. To determine  $T_c$  very accurately for such a small anisotropy one would need accurate data for even larger system sizes. However, the current precision is enough for the comparisons with results of approximate theoretical methods that we present in the next section.

## B. Magnetization

We compare the QMC data with Schwinger Boson mean-field<sup>13</sup> and many-body Green's functions calculations.<sup>10,11</sup> Both methods include spin wave excitations approximately and represent significant improvements over simple mean field theories in which magnon excitations are neglected completely. Of these two methods the Schwinger boson theories are numerically less demanding and much easier to extend to arbitrary spin than the RPA approach.<sup>13</sup>

In the Schwinger boson theory the Heisenberg model is mapped onto an equivalent bosonic system. This can be done by using the  $SU(2)$  symmetry in spin space of the Heisenberg model. The  $SU(2)$  model can then be generalized to an  $SU(N)$  model, containing  $N$  bosons per site. In the limit  $N \rightarrow \infty$  mean-field theory becomes exact, and in this section we label mean-field  $SU(N \rightarrow \infty)$  results by “ $SU(N)$ ”. Using the local equivalence between

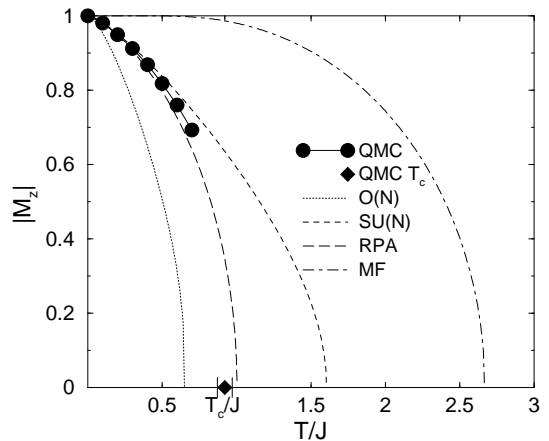


FIG. 8: Magnetization as a function of temperature  $T/J$  for  $S = 1$  and  $K_2/J = 0.01$ .

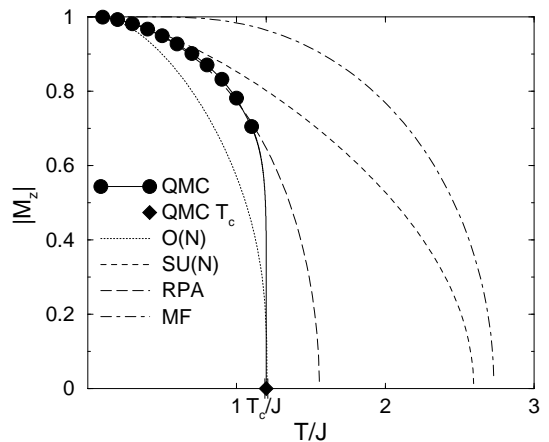


FIG. 9: Magnetization as a function of temperature  $T/J$  for  $S = 1$  and  $K_2/J = 0.20$ .

the  $SU(2)$  and  $O(3)$  groups, this can be repeated for an  $O(3)$  model, and we label mean-field  $O(N \rightarrow \infty)$  results by “ $O(N)$ ”.

The many-body Green's function calculations for the magnetization are done by a procedure where one works at the second level of the hierarchy of equations of motion for the Green's functions.<sup>11</sup> This allows an exact treatment of the terms stemming from the single-ion anisotropy, whereas the exchange interaction terms are treated by the Tyablicov<sup>16</sup>, or random-phase approximation (RPA), and from now on Green's function results will be labeled by RPA. This procedure is an improvement over the Anderson-Callen decoupling<sup>10</sup>, in which the single-ion anisotropy terms are decoupled at the level of the lowest-order equation of motion, which is a good approximation only for small anisotropies.<sup>11</sup> The results in this subsection are calculated using the exact treatment of the single-ion anisotropy. Owing to problems with numerical stability, the calculations for the reorien-

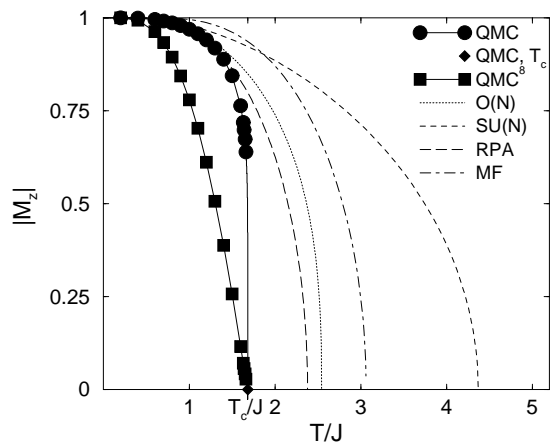


FIG. 10: Magnetization as a function of temperature  $T/J$  for  $S = 1$  and  $K_2/J = 1.50$ .

tation of the magnetization discussed in the next subsection are done with the Anderson-Callen decoupling.

We compare magnetization curves for three values of the anisotropy covering three orders of magnitude,  $K_2/J = 0.01, 0.2$  and  $1.5$ . The smallest value is of greatest relevance for experiments, but it is of interest to see how well the analytic methods work outside this region as well. In Fig. 8 we see that, for  $K_2/J = 0.01$  the RPA calculations give a rather accurate magnetization curve, while the  $O(N)$  and  $SU(N)$  theories give a low and high estimate, respectively. In the low-temperature limit both the  $SU(N)$  theory and the RPA calculation recover the correct spin-wave result. Note also by how much a simple mean-field (MF) theory overestimates the magnetization ( $T_c^{\text{MF}} \simeq 2.7 T_c^{\text{QMC}}$ !). As is well known, mean-field theory also totally fails at low temperatures (exponential instead of power law behaviour), due to the neglect of spin waves. In Fig. 9 we see that for  $K_2/J = 0.2$  the RPA still gives very accurate values at low temperatures, while overestimating the magnetization at higher temperatures. The  $O(N)$  theory happens to give a good estimate of  $T_c$ , while the  $SU(N)$  again overestimates the magnetization. In Fig. 9 the QMC points are connected by straight lines, except for the line between  $T_c$  and the highest temperature below  $T_c$ . This line is a fit to the Ising-like critical behavior

$$M_z \propto (T - T_c)^{\frac{1}{8}}. \quad (14)$$

The good fit indicates that the QMC data have come close enough to  $T_c$  for the critical behavior to set in. For the largest anisotropy,  $K_2/J = 1.5$  (Fig. 10), the RPA calculation again gives the most accurate estimate, but all approximate curves result in too high a magnetization. For high temperatures the  $SU(N)$  theory yields a larger magnetization than simple mean-field theory. In Fig. 10 we have also included the quantum Monte Carlo data raised to the eighth power. The resulting straight line is further evidence of how close to the critical point the

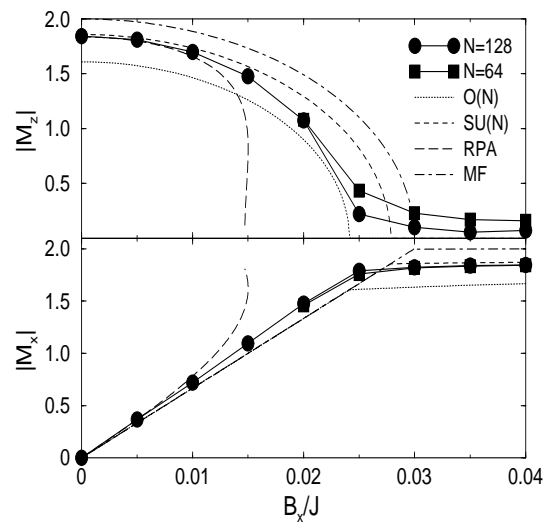


FIG. 11: In-plane and out-of-plane magnetization as a function of transverse field at temperature  $T/J = 1$  for  $S = 2$ ,  $K_2/J = 0.01$ .

simulation has come.

The large deviations of the approximate theoretical treatments from QMC, in particular close to  $T_c$  and for large anisotropies, indicate that neither the Green's function approach nor the Schwinger boson method treats spin wave interactions in a satisfactory way. It is interesting to note that that RPA and  $SU(N)$  give a (mean-field) exponent of  $1/2$ , whereas  $O(N)$  gives  $1/3$ .

In this subsection we have compared QMC data with approximate theoretical results for the magnetization curve. Except for the value of  $T_c$ , the QMC data shown above have converged in system size within error bars that are not discernible in the figures. The largest system size used is  $256 \times 256$  spins. Error bars are shown for the Binder estimate of  $T_c$ . As can be seen the error increases with decreasing anisotropy, which is to be expected.

### C. Reorientation

We consider two examples for the reorientation of the magnetization in a transverse field. For an anisotropic spin-2 model we have calculated the vertical and transverse components of the magnetization,  $M_z$  and  $M_x$ , as a function of a transverse magnetic field at a fixed temperature.

The anisotropy favors an out-of-plane magnetization, while the transverse field wants the magnetization to be in the plane. This competition results in quite interesting phase diagrams, where the order of the transition in general depends on the order of the anisotropy.<sup>13</sup> Here we concentrate on two examples, to demonstrate the applicability of the QMC approach.

In Fig. 11 we show the magnetization curves for a small

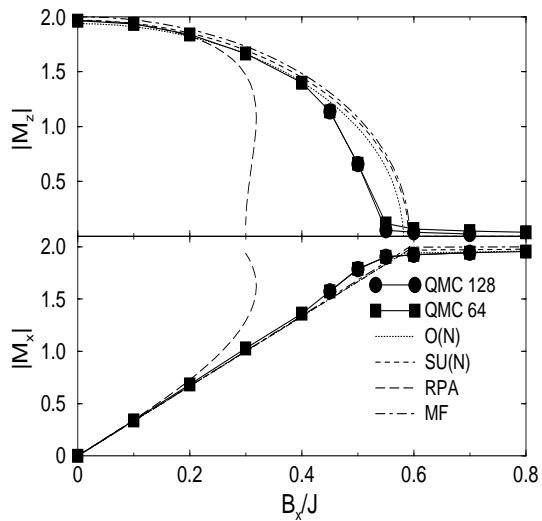


FIG. 12: In-plane and out-of-plane magnetization as a function of transverse field at temperature  $T/J = 1$  for  $S = 2$ ,  $K_2/J = 0.2$ .

anisotropy,  $K_2/J = 0.01$ , at a temperature  $T/J = 1$ . Primarily we show QMC results for system size  $128 \times 128$ , but in addition we show results for  $64 \times 64$  in the region where they differ from each other. For small and intermediate fields the results have converged, while we again see increasing finite-size effects closer to the critical field. The trend is, however, clear. The transverse magnetization does appear to increase linearly with the transverse field, up to the highest fields for which the results have converged.

The  $SU(N)$  and  $O(N)$  calculations both show a linear dependence on the transverse magnetization,  $M_x$ , similar to QMC, whereas the vertical component is over- or underestimated, respectively. The  $SU(N)$  results for  $M_z$  are good at weak field, though. The mean-field results for  $M_x$  are also linear but mean-field theory consistently overestimates  $M_z$ . The RPA calculation with the approximate decoupling of the anisotropy terms<sup>10</sup> follows the QMC curves at small values of the transverse field, but the reorientation occurs at a considerably smaller critical field than in QMC and in the other approximations. Also, in the RPA the magnetization is not a unique function of field close to the transition. The same system has been studied for a larger anisotropy,  $K_2/J = 0.20$ , in Fig. 12. Here the  $SU(N)$  and  $O(N)$  solutions are mean-field-like and agree very well with the QMC solution, except close to the transition, whereas the RPA behaves as in Fig. 11. Close to the transition the  $SU(N)$ ,  $O(N)$ , and mean-field solutions overestimate the vertical magnetization. The

QMC results display a small deviation from the linear increase in the in-plane magnetization, which is not reproduced by the Schwinger boson or mean-field methods.

#### IV. CONCLUSION

This work shows the feasibility of using large-scale QMC calculations to examine microscopic thin film models. The QMC approach can be used both as a sanity check on approximate theoretical treatments and as a method in its own right. Our results indicate that in the absence of a transverse field, RPA with an exact treatment of the anisotropy terms<sup>11</sup> appears to be more accurate than the Schwinger boson calculation. Both methods, however, represent an improvement over simple mean-field theory for small anisotropies but QMC reveals weaknesses in the approximate theories at large anisotropies and close to the Curie temperature. In the presence of a transverse field the results obtained from Schwinger boson methods are quite mean-field-like, which turns out to be appropriate for most of the field range. The reason that the RPA is worse in this case is probably due to the Anderson-Callen decoupling of the anisotropy terms in RPA.<sup>10</sup> This was necessary because the more accurate treatment<sup>11</sup> led to numerical difficulties when applied to the reorientation problem. To make more definite conclusions about the merits of different approximate methods, we would have to investigate a much larger parameter space, including higher anisotropies, general spin, temperature, and transverse field and the extension to several layers. We leave such an investigation as work for the future.

It is possible to extend the QMC calculations to include several layers with arbitrary inter-layer coupling, as well as, for example, anisotropies in the exchange coupling. Unfortunately, the dipole interaction introduces frustration and thereby the sign problem, and is therefore currently out of reach for QMC studies. On the other hand, long-range ferromagnetic couplings are not a problem. The implementation of the dipole coupling also leads to problems in the Schwinger boson theory but is possible in a Green's function description.<sup>7,10</sup> A very exciting recent development in QMC is the introduction of directed loop moves,<sup>24</sup> which, according to our initial calculations, can reduce the autocorrelation time by one order of magnitude in spin-1 systems, and therefore make it possible to reach substantially larger system sizes. However, it is not clear that the directed loops are as easy to implement for a general model as the method used in this work.

We are grateful to A. Sandvik for fruitful discussions. P.H. acknowledges support by the Swedish Research Council and Ella och Georg Ehrnrooths stiftelse.

\* Electronic address: patrik@theophys.kth.se

<sup>1</sup> J. A. C. Bland and B. Heinrich, *Ultrathin Magnetic Structures* (Springer-Verlag, Berlin, 1994).

<sup>2</sup> O. Hjortstam, K. Baberschke, J. M. Wills, B. Johansson, and O. Erickson, *Phys. Rev. B* **55**, 15026 (1997).

<sup>3</sup> A. Moschel and K. D. Usadel, *Phys. Rev. B* **49**, 12868



- (1994).
- <sup>4</sup> P. J. Jensen and K. H. Bennemann, in *Magnetism and Electronic Correlations in Local-Moment Systems: Rare-Earth Elements and Compounds*, edited by M. Donath, P. A. Dowben, and W. Nolting (World Scientific, Singapore, 1998).
  - <sup>5</sup> R. P. Erickson and D. L. Mills, *Phys. Rev. B* **43**, 11527 (1991).
  - <sup>6</sup> O. Iglesias, A. Valencia, and A. Labarta, *J. Magn. Magn. Matter* **196-197**, 819 (1999).
  - <sup>7</sup> P. J. Jensen, K. H. Bennemann, P. Pouloupoulos, M. Farle, F. Wilhelm, and K. Baberschke, *Phys. Rev. B* **60**, R14884 (1999).
  - <sup>8</sup> A. Ecker, P. Fröbrich, P. J. Jensen, and P. J. Kuntz, *J. Phys. Cond. Matter* **11**, 1557 (1999).
  - <sup>9</sup> P. Fröbrich, P. J. Jensen, and P. J. Kuntz, *Eur. Phys. J. B* **13**, 477 (2000).
  - <sup>10</sup> P. Fröbrich, P. J. Jensen, P. J. Kuntz, and A. Ecker, *Eur. Phys. J. B* **18**, 579 (2000).
  - <sup>11</sup> P. Fröbrich, P. J. Kuntz, and M. Saber, *Ann. Physik* **11**, 387 (2002).
  - <sup>12</sup> R. P. Erickson and D. L. Mills, *Phys. Rev. B* **44**, 11825 (1991).
  - <sup>13</sup> C. Timm and P. J. Jensen, *Phys. Rev. B* **62**, 5634 (2000).
  - <sup>14</sup> C. Timm, S. M. Girvin, P. Henelius, and A. W. Sandvik, *Phys. Rev. B* **58**, 1464 (1998).
  - <sup>15</sup> P. Henelius, A. W. Sandvik, C. Timm, and S. M. Girvin, *Phys. Rev. B* **61**, 364 (2000).
  - <sup>16</sup> S. V. Tyablicov, *Ukr. Mat. Zh.* **11**, 287 (1959).
  - <sup>17</sup> A. W. Sandvik, *Phys. Rev. B* **59**, R14157 (1999).
  - <sup>18</sup> A. W. Sandvik and J. Kurkijärvi, *Phys. Rev. B* **43**, 5950 (1991).
  - <sup>19</sup> N. V. Prokof'ev, B. V. Svistunov, and I. S. Tupitsyn, *Pis'ma Zh. Eks. Teor. Fiz.* **64**, 853 (1996).
  - <sup>20</sup> B. B. Beard and U.-J. Wiese, *Phys. Rev. Lett.* **77**, 5130 (1996).
  - <sup>21</sup> S. M. A. Rombouts, K. Heyde, and N. Jachowicz, *Phys. Rev. Lett.* **82**, 4155 (1999).
  - <sup>22</sup> H. G. Evertz, G. Lana, and M. Marcu, *Phys. Rev. Lett.* **70**, 875 (1993).
  - <sup>23</sup> N. Kawashima, J. E. Gubernatis, and H. G. Evertz, *Phys. Rev. B* **50**, 136 (1994).
  - <sup>24</sup> O. F. Syljuåsen and A. W. Sandvik, cond-mat/0202316.
  - <sup>25</sup> P. Henelius and A. W. Sandvik, *Phys. Rev. B* **62**, 1102 (2000).
  - <sup>26</sup> N. D. Mermin and H. Wagner, *Phys. Rev. Lett.* **17**, 1133 (1966).
  - <sup>27</sup> M. Bander and D. L. Mills, *Phys. Rev. B* **38**, 12015 (1988).
  - <sup>28</sup> K. Binder, *Z. Phys B* **43**, 119 (1981).